Multivariate Statistical Analysis of Two-Dimensional Metal Cluster Arrays Grown in Vitro on a Bacterial Surface Layer

Reiner Wahl,[†] Harald Engelhardt,[‡] Wolfgang Pompe,[†] and Michael Mertig*[,†]

Max Bergmann Zentrum für Biomaterialien and Institut für Werkstoffwissenschaft, Technische Universität Dresden, D-01069 Dresden, Germany, and Max-Planck-Institut für Biochemie, D-82152 Martinsried, Germany

Received September 5, 2004. Revised Manuscript Received January 10, 2005

Regular nanocluster arrays were fabricated by chemical reduction of Pd complexes in the presence of the two-dimensional crystalline surface layer protein from the bacterium *Sporosarcina ureae*. The size of Pd clusters grown on the protein, its occupation properties, and the local cluster distribution on the protein surface were analyzed by electron microscopy, correlation averaging, and multivariate statistical analysis. The Pd clusters of 1.2−1.5 nm in size are preferably located in and close to pores and gaps of the protein framework in seven cluster sites of three different types per unit cell. The sites are almost completely occupied. The clusters appear strongly directed by the protein template but show positional variability within the main cluster sites. This variability is an inherent property of the Pd clusters and cannot be explained by statistical error with positional analysis. Binding studies with Pd complexes prior to reduction suggested that a high number of potential nucleation sites are formed on the protein surface, facilitating the initial growth of clusters at variable positions. A model for heterogeneous nucleation and cluster development on protein surfaces is proposed and compared to the mechanism of reductive metallization of DNA investigated previously.

1. Introduction

The application of biomolecular structures as templates for the controlled organization of inorganic matter at the nanometer scale is a very promising approach to the development of reliable bottom-up strategies for the formation of low-dimensional hybrid materials with novel electronic, optical, or chemical properties. Advanced nanostructure fabrication by biomolecular templating takes advantage of the recognition and self-assembly properties of biomolecules, which allow a tailored formation of DNA or protein templates with pre-defined geometries[1−4] and spatially defined physical and chemical surface properties. Several methods of metal application have been used, the most important being metal deposition in vacuo by metal shadowing or decoration,[5−7] deposition of preformed metal particles, e.g., gold, in aqueous solution,[8−10] and, more recently, growth of metal clusters generated by chemical redox mineralization processes in vitro starting from template-bound metal complexes.[11−16]

Regularly arrayed protein structures such as bacterial and archaeal surface layers (S layers) with lattice constants of 5−30 nm are of particular interest for the in vitro formation of metal arrays in two dimensions. S layers are natural two-dimensional (2D) crystalline protein sheets found in the cell envelope of bacteria and archaea.[17] They usually form the outermost cell wall layer and represent the only cell wall component in many archaea. S-layer proteins are arranged in *p*2, *p*3, *p*4, and *p*6 symmetries and exhibit distinctly different structures and properties at the extracellular (outer) surface oriented toward the surrounding medium and the cellular (inner) surface associated with the underlying cell envelope component.[18] The protein crystals usually show several pores and gaps per unit cell that have significance for macromolecules to penetrate.[19] S layers exhibit variable

* To whom correspondence should be addressed. Phone: +49-351-463-39404. Fax: +49-351-463-39401. E-mail: mertig@tmfs.mpgfk.tu-dresden.de.
[†] Technische Universität Dresden.
[‡] Max-Planck-Institut für Biochemie.

(1) Yan, H.; Park, S. H.; Finkelstein, G.; Reif, J. H.; LaBean, T. H. *Science* **2003**, *301*, 1882.
(2) Seeman, N. C. *Curr. Opin. Struct. Biol.* **1996**, *6*, 519.
(3) Baumeister, W.; Wildhaber, I.; Engelhardt, H. *Biophys. Chem.* **1988**, *29*, 39.
(4) Györvary, E.; O'Riordan, A.; Quinn, A.; Redmond, G.; Pum, D.; Sleytr, U. B. *Nano Lett.* **2003**, *3*, 315.
(5) Winkler, H.; Wildhaber, I.; Gross, H. *Ultramicroscopy* **1985**, *16*, 331.
(6) Bachmann, L.; Weinkauf, S.; Baumeister, W.; Wildhaber, I.; Bacher, A. *J. Mol. Biol.* **1989**, *207*, 575.
(7) Pompe, W.; Mertig, M.; Kirsch, R.; Engelhardt, H.; Kronbach, T. Functionalized biomolecular membranes for microreactors. In *Microreaction Technology - Proceedings of the First International Conference on Microreaction Technology*; Ehrfeld, W., Ed.; Springer-Verlag: Berlin-Heidelberg-New York, 1998; p 104.
(8) Elghanian, R.; Storhoff, J. J.; Mucic, R. C.; Letsinger, R. L.; Mirkin, C. A. *Science* **1997**, *277*, 1078.
(9) Alivisatos, A. P.; Johnson, K. P.; Peng, X.; Wilson, T. E.; Loweth, C. J.; Bruchez, M. P. Jr.; Schultz, P. G. *Nature* **1996**, *382*, 609.
(10) Hall, S. R.; Shenton, W.; Engelhardt, H.; Mann, S. *ChemPhysChem* **2001**, *3*, 184.
(11) Braun, E.; Eichen, Y.; Sivan, U.; Ben-Yoseph G. *Nature* **1998**, *391*, 775.
(12) Richter, J.; Seidel, R.; Kirsch, R.; Mertig, M.; Pompe, W.; Plaschke, J.; Schackert, H. K. *Adv. Mater.* **2000**, *12*, 507.
(13) Mertig, M.; Colombi Ciacchi, L.; Seidel, R.; Pompe, W.; De Vita, A. *Nano Lett.* **2002**, *2*, 841.
(14) Shenton, W.; Pum, D.; Sleytr, U. B.; Mann, S. *Nature* **1997**, *389*, 585.
(15) Mertig, M.; Kirsch, R.; Pompe, W.; Engelhardt, H. *Eur. Phys. J. D* **1999**, *9*, 45.
(16) Mertig, M.; Wahl, R.; Lehmann, M.; Simon, P.; Pompe, W. *Eur. Phys. J. D* **2001**, *16*, 317.
(17) Beveridge, T. J.; Graham, L. L. *Microbiol. Rev.* **1991**, *55*, 684.
(18) Engelhardt, H.; Peters, J. *J. Struct. Biol.* **1998**, *124*, 276.

10.1021/cm048497p CCC: $30.25
Published on Web 03/08/2005

structures in detail[20−22] and some of them remarkable stability even under extreme conditions,[18] features that make them attractive templates for metal deposition.[7,10,14−16,23−25] The obvious correlation between the spatial distribution of metal clusters and the geometry of the protein target led to the hypothesis of a template-controlled metal deposition at specific sites. However, the specific functionalities of such affinity sites, e.g., the spatial organization of charged or hydrophobic residues, the presence of reactive (chelating, reducing, or oxidating) groups, or the location of modified (glycosylated) amino acids, are still unknown for S layers, mainly because of the lack of high-resolution structures.

One possible approach to obtain more information about the local affinity sites of S-layer surfaces is to analyze the individual metal cluster positions by means of electron microscopy and image processing. These methods allow the study of both the characteristic cluster positions and their local variability. Previous investigations on platinum arrays using image-averaging methods already revealed preferred sites for cluster formation on the S-layer surface.[15] However, contrast differences between the various cluster sites also indicated remarkable variations in the deposition of metal clusters. The exact topography of individual clusters and its relation to the S-layer template has not been analyzed so far, but it can be expected to provide valuable information on the properties of cluster-protein interactions.

Here we study a system consisting of a palladium cluster array grown on the S layer from the bacterium *Sporosarcina ureae*.[26] Our focus is the analysis of individual metal cluster positions with the aim to get a deeper insight into the distribution and local properties of individual affinity sites and to shed some light on the template-controlled nucleation and growth processes, which are not yet understood at the molecular level. We apply principal component analysis (PCA), a variant of correspondence analysis that has been proven to a be a powerful tool for elucidating structural characteristics and variability in electron microscopical images from various applications.[27−32]

2. Materials and Methods

2.1. Sample Preparation. The S layer was isolated from the bacterium *Sporosarcina ureae* (ATCC 13881). The conditions for cell cultivation and purification of S-layer sheets were described previously.[26] Pd cluster arrays were grown on the 2D crystalline protein by a method similar to that for the metallization with Pt as described by Mertig et al.[15] To this end, 50 μL of an S-layer suspension (7.5 mg/mL protein in buffer solution: 50 mM KH_2PO_4/Na_2HPO_4, pH 7.5, 1 mM $MgCl_2$, 3 mM NaN_3) were mixed with 1 mL of a 3 mM K_2PdCl_4 solution; the latter had been prepared 24 h before to enable hydrolysis of the metal complexes.[33] After 24 h, 50 μL of the sample was diluted in 1 mL of bidest H_2O, and this solution was used for electron microscopy.

2.2. Binding of Pd Complexes to the S-Layer Protein without Reduction and Cluster Formation. To estimate how many unreduced metal complexes bind to the S-layer protein during incubation prior to the reduction process, aliquots (50 μL) of an S-layer preparation, containing 10 mg/mL protein in Tris/H_2SO_4 pH 7.4, were dissolved in 1 mL of a 24-h-aged solution of K_2PdCl_4 (3 mM). After incubation at 25 °C for 1 h, the S-layer protein was removed by ultracentrifugation at 4 °C for 1 h and the supernatant used for UV−vis spectroscopy. Spectra were recorded from 300 to 700 nm and analyzed as described.[34] The amount of Pd complexes bound to the S layer was calculated in comparison to control experiments with K_2PdCl_4 solutions free of protein.

2.3. Transmission Electron Microscopy (TEM). A droplet of about 5−10 μL of the sample solution, prepared as described in section 2.1, was placed onto a carbon-coated copper grid that had been made hydrophilic by glow discharge. Excess liquid was blotted with filter paper, and the sample immediately washed by placing the grid onto a 500-μL drop of water. The grid was blotted and the sample air dried.

Electron microscopy was carried out in low-dose mode using a Philips CM 12 equipped with a LaB_6 cathode. The sample was exposed to the electron beam only during image recording to avoid radiation damage. All the focusing and image inspections were performed with areas neighboring those of interest. Images were recorded by means of a charge-couple device camera (1024 pixels × 1024 pixels) at 500-ms exposure time. For detailed analyses, a series of partially overlapping images of an S-layer sheet was recorded at a primary magnification of 100 000×, corresponding to a pixel size of 0.12 nm on the specimen level.

2.4. Image Analysis. In the first step, the TEM images of metal cluster arrays were analyzed by correlation averaging[35] using the SEMPER image-processing system[36] installed on an SGI workstation. To obtain a noise-reduced reference for subsequent cross correlation, each of the images of the metallized S layer was Fourier transformed and window filtered such as to select the reflections containing the periodic information of the 2D crystal only. The transform was high- and low-pass filtered in addition to remove insignificant reflection spots.[37] A reference of 2 × 2 unit cells in size was extracted from the back transformed image for cross correlation and determination of the unit cell positions in the original image. The use of such almost noise-free reference images with an optimized signal-to-noise ratio promises least error positioning of the individual unit cells in the original images of (imperfect) 2D crystals. This procedure also limits the error of unit cell centering introduced by the variable distribution of metal clusters within the unit cells. Since the individual distribution of clusters is not compared to another original unit cell image but with the average distribution (e.g., density) of clusters, the definition of the particular

(19) Sára, M.; Sleytr, U. B. *J. Bacteriol.* **2000**, *182*, 859.
(20) Sleytr, U. B.; Messner, P. *J. Bacteriol.* **1988**, *170*, 2891.
(21) Baumeister, W.; Wildhaber, I.; Phipps, B. M. *Can. J. Microbiol.* **1989**, *35*, 215.
(22) Rachel, R.; Pum, D.; Smarda, J.; Smajs, D.; Komrska, J.; Krzyzánek, V.; Rieger, G.; Stetter, K. O. *FEMS Microbiol. Rev.* **1997**, *20*, 13.
(23) Douglas, K.; Clark, N. O.; Rothschild, K. J. *Appl. Phys. Lett.* **1990**, *56*, 692.
(24) Dieluweit, S.; Pum, D.; Sleytr, U. B. *Supramol. Sci.* **1998**, *5*, 15.
(25) Wahl, R.; Mertig, M.; Raff, J.; Selenska-Pobell, S.; Pompe, W. *Adv. Mater.* **2001**, *13*, 736.
(26) Engelhardt, H.; Saxton, W. O.; Baumeister, W. *J. Bacteriol.* **1986**, *168*, 309.
(27) Frank, J.; van Heel, M. *J. Mol. Biol.* **1982**, *161*, 134.
(28) Engelhardt, H.; Guckenberger, R.; Hegerl, R.; Baumeister, W. *Ultramicroscopy* **1985**, *16*, 395.
(29) Frank, J. *J. Electron Microsc. Rev.* **1989**, *2*, 53.
(30) Akey, C. W. *J. Mol. Biol.* **1995**, *248*, 273.
(31) Aebersold, J. F.; Stadelmann, P. A.; Rouvière, J.-L. *Ultramicroscopy* **1996**, *62*, 171.
(32) Braun, N.; Tack, J.; Bachmann, L.; Weinkauf, S. *Thin Solid Films* **1996**, *284−285*, 703.
(33) Henglein, A.; Ershov, B. G.; Malow, M. *J. Phys. Chem.* **1995**, *99*, 14129.
(34) Wahl, R. Dissertation, Technische Universität Dresden, 2003.
(35) Saxton, W. O.; Baumeister, W. *J. Microsc.* **1982**, *127*, 127.
(36) Saxton, W. O. *J. Struct. Biol.* **1996**, *116*, 230.
(37) Engelhardt, H. *Methods Microbiol.* **1988**, *20*, 357.

unit cell center is least impaired. In addition, the contribution of pure protein contrast is enhanced in the Fourier-filtered and in the averaged references, improving the positioning of unit cells further.

In a second run, the cross correlation was refined with the result from correlation averaging as a new reference. Averages and variance images of the unit cells were calculated and the position coordinates used to extract images of the unit cells. These were re-sampled with respect to the base vectors in order to fit the unit cells of the *p*4 lattice into square images of dimensions $a = b =$ 12.9 nm (108 pixels × 108 pixels). Double peaks from overlapping regions were removed from the peak list. In addition, unit cells located close to the border of the metallized S layer, and those situated in double-layer areas of the partially folded S-layer sheet, were excluded. The remaining coordinate list contained $N = 420$ unique positions of unit cells being centered on the minor 4-fold symmetry axis according to the nomenclature of Engelhardt et al.[28] These unit cell images were used for multivariate statistical analyses.

Principal component analysis (PCA)[27,31] was performed by means of the EM image processing system.[38] The images of unit cells or extracted subframes thereof were normalized to a mean value of 0 and a standard deviation of 1. Prior to PCA, the average of all images was subtracted from the individual ones. The 10 most significant eigenvectors (eigenimages) and the corresponding importance images were calculated. For classification, the first *Q* eigenimages were selected and the coordinates of the individual images in *N*-dimensional space ($N = 420$) projected into the *Q*-dimensional subspace.

2.5. Statistical Analysis of Cluster Displacements. Local variations in cluster positions in identical metallization sites from different unit cells may originate from misalignment or from other sources. To distinguish between these situations, the cluster positions of the four equivalent metallization sites (protein pores) located around the minor 4-fold symmetry axis[26] were investigated separately. The analysis is based on the fact that the cluster positions in the four sites become correlated if the unit cell was displaced upon misalignment, i.e., the cluster positions were shifted in the same direction. The $N = 420$ cluster positions per individual A site (A_1 to A_4) were analyzed by PCA and separated into six subsets, using the most significant five eigenvectors for classification. In the next step, the unit cells UC_i were identified that contributed to the $N_{1,A1}$ ($N_{2,A1}$, $N_{3,A1}$, ..., $N_{6,A1}$) clusters in class #1 (#2, #3, ..., #6) of site A_1. Now, the corresponding N_1 images of site A_2 (A_3, A_4), identified by the same unit cell numbers, were selected and determined how many clusters had been distributed to the classes #1−6 of this site upon independent PCA and corresponding classification. The hypothesis (H_0) is that the observed frequencies are statistically identical to the expected frequencies derived from the distribution of the 420 images to the six classes of site A_2 (A_3, A_4). The expected frequencies are $N_{1,A1}{\cdot}N_{1,A2}/420$ ($N_{1,A1}{\cdot}N_{2,A2}/420$, ..., $N_{1,A1}{\cdot}N_{6,A2}/420$) for the six classes of site A_2 according to the $N_{1,A1}$ images regarded. The other frequencies are calculated accordingly. The expected and the real distributions were compared by χ^2 tests (degrees of freedom = 5 for each test) and the results judged according to a significance level of 5%. The clusters are regarded as not correlated if the tests revealed a probability of >0.05.

3. Results

3.1. Image Analysis of Pd Cluster Arrays by Correlation Averaging. The treatment of the S-layer template with palladium complexes (K_2PdCl_4) led to the development of Pd cluster arrays in a similar way as obtained for platinum previously.[15] Figure 1 shows a compilation of overlapping micrographs taken from a single S-layer sheet after metallization. Each of the subframes was recorded at low-dose conditions and possesses a size of 123-nm square, corresponding to an area of about 90 unit cells with *p*4 symmetry and lattice constants of $a = b = 12.9$ nm. The subframes contained 420 unique unit cells that were identified by means of cross correlation. These unit cells were used for averaging and multivariate statistical analysis.

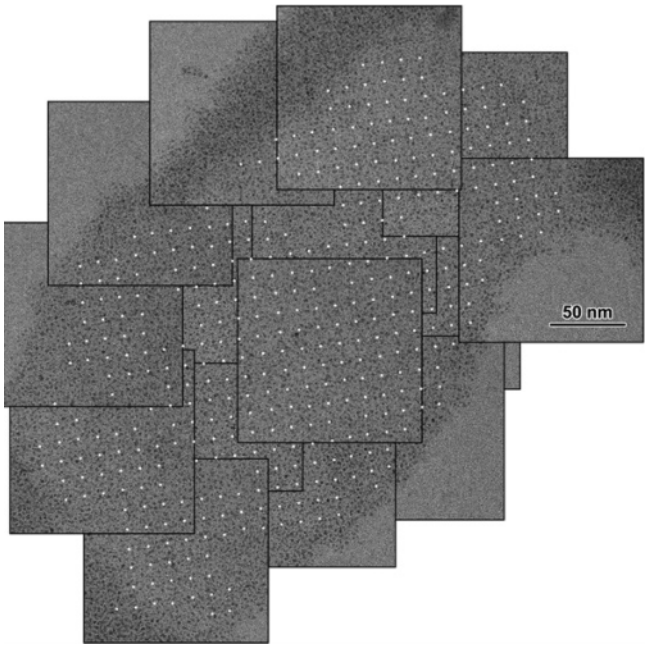

Figure 1. Electron micrograph of a Pd cluster array grown on the S layer of *Sporsarcina ureae*, exhibiting a *p*4 lattice with a lattice constant of 12.9 nm. The image is a compilation of partially overlapping micrographs (subframes indicated) taken from a single metallized S-layer sheet. The positions of the 420 individual unit cells that were extracted from the micrographs and used for averaging and multivariate statistical analysis are marked with white dots. These indicate the centers of the minor 4-fold symmetry axes as identified in Figure 2. Metal clusters grown on the protein surface are identified as small dark spots.

Correlation averaging revealed the distribution of clusters on the protein template on average (Figure 2). In the following, we distinguish between "cluster sites", i.e., subareas of the unit cell exhibiting increased metal contrast as obtained by averaging, and "cluster positions", referring to the individual positions of metal particles (Pd clusters), e.g., within these sites.

Although the contrast of protein is low in electron micrographs, the structure of unstained S layers can be rendered visible and reliably be reconstructed in 2D and in 3D.[39−41] The average in Figure 2C clearly reveals the basic structural domains of the S-layer unit cells and shows that the preferred cluster sites coincide with the pore regions of the S-layer topography. The size, shape, and location of high contrast areas in Figure 2C (indicating metal) match the geometry of pores and gaps of the protein network (Figure 2A). These pores belong to three different types (Figure 2): four identical pores around the minor 4-fold symmetry axis of the unit cell (type A), elongated gaps at the 2-fold

(38) Lepault, J.; Pitt, T. *EMBO J.* **1984**, *3*, 101.
(39) Hegerl, R. *J. Struct. Biol.* **1996**, *116*, 30.
(40) Baumeister, W. *Curr. Opin. Struct. Biol.* **2002**, *12*, 679.
(41) Simon, P.; Lichte, H.; Wahl, R.; Mertig, M.; Pompe, W. *Biochim. Biophys. Acta* **2004**, *1663*, 178.

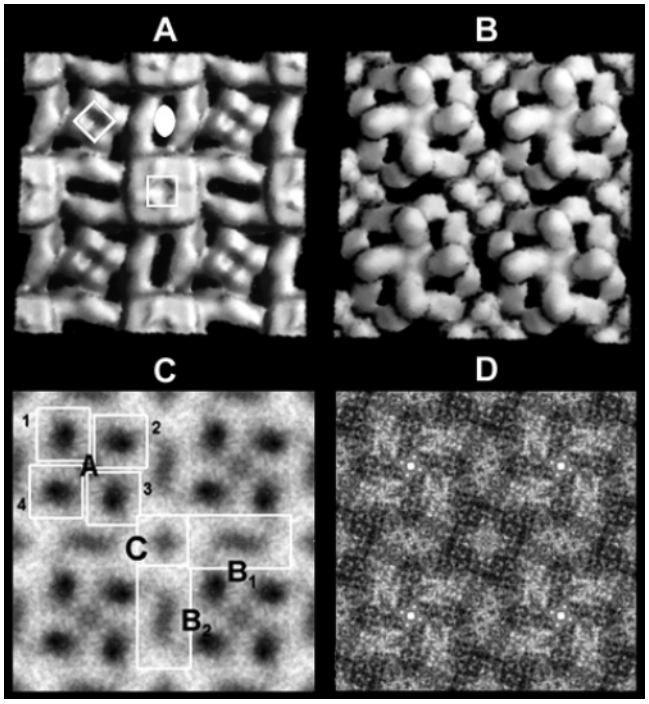

Figure 2. (A and B) Model of the S layer from *S. ureae* obtained by surface rendering of the 3D data set from a negatively stained preparation.[24] (A) Inner surface, crystallographic symmetry axes: ◇, minor 4-fold symmetry axis, () 2-fold symmetry axis, and □ major 4-fold symmetry axis. (B) Outer surface. (C) Correlation average of the 420 unique positions of unit cells, representing the mean distribution and the preferred sites of Pd clusters (dark) grown on the S-layer surface. Characteristic cluster sites at the symmetry axes are marked: four equivalent clusters are located at sites A_1-A_4, two at sites B_1 and B_2, and one at site C. (D) Variance image depicting structural variability among the averaged units cells. Bright areas indicate variable contrast in the images. Size of images 2 × 2 unit cells, corresponding to 25.8 × 25.8 nm^2.

symmetry axes (type B), and a porelike indentation at the major 4-fold symmetry axis (type C). At least the latter represents a combined position from the inner and the outer surface of the S layer (parts A and B of Figure 2), which are not differentiated in the 2D projections of our analysis. As shown in Figure 2C, four equivalent cluster sites with strong contrast are located at position A. Apparently, an elongated cluster site is found at the 2-fold symmetry axis (position B) and another cluster area is located at position C. The site at the minor 4-fold symmetry axis in A is another potential cluster site but was excluded from further analysis because of poor contrast and high variability according to the variance image in Figure 2D. Thus, from a crystallographic point of view, each of the unit cells contains 7 major distinguishable cluster sites in projection, i.e., four around position A, two at position B, and one at position C. The cluster sites found here are identical to the positions for platinum clusters grown on the same S layer as reported previously.[15]

The cluster sites exhibited remarkable differences in their density contrast (Figure 2C). This gives rise to the assumption that the cluster sites were either variably occupied from one unit cell to the next or that the positions of individual Pd particles differed notably. So, it is impossible to judge whether the protein gap at site B is filled with one elongated metal cluster or with smaller clusters variously positioned along the pore. The variance image (Figure 2D) suggests similar degrees of variability for all the cluster sites (A to C) but it does not provide information on the nature of variance. To study the contributions of cluster shape, position, and frequency to variable site occupation, we applied PCA.

3.2. Multivariate Statistical Analysis of Unit Cells. In a first attempt, we analyzed the distribution of metal clusters at the level of whole unit cells by PCA. The resulting eigenvectors did not reveal clear structural differences between individual unit cells, which should show up by prominent contrast variations. We must therefore assume that each unit cell contained a number of metal clusters that contributed individually and independently to structural or statistical variability, so that no particular distribution of metal clusters was dominating. In the following, we divided the unit cells into subareas according to the preferred metallization sites A−C and subjected them to PCA independently.

3.3. Multivariate Statistical Analysis of Individual Metallization Sites. According to the identification of different cluster sites per unit cell, we selected seven subareas for individual PCA (Figure 2C). The subareas were centered at the corresponding sites and were about twice as wide as the apparent clusters. Since the four areas at position A and the two at B, respectively, are crystallographically equivalent, we combined them to coherent data sets. The images A_2-A_4 were rotated by $\pi/2$, π, and $-\pi/2$, respectively, to align the structures with respect to the subframe A_1. In the same way, the subareas at position B were combined, rotating area B_2 by $\pi/2$. The resulting three data sets comprised 1680 images for the cluster sites at A, 840 images for sites B, and 420 images for C, the latter without any rotational correction. The positional error possibly introduced by extraction and rotation of the subframes should not exceed 1 pixel or 0.12 nm.

As an example, Figure 3 shows the total average and the 10 most significant eigenvectors (out of 1679) of data set A processed by PCA. The first 10 eigenimages already accounted for 15.6% of the total variance but with relatively small differences between the eigenvalues of consecutive eigenvectors. They describe the most important (and independent) contrast variations (originating from metal contrast) in the images of the data set. The so-called "importance images" depicted in Figure 3 help to illustrate the theoretical extremes of the structural image characteristics calculated from the corresponding eigenvectors (but they do not represent real images). Accordingly, the first eigenvector (Figure 3, #1) distinguishes between images containing centered Pd clusters in a metal-free surrounding and the opposite situation, i.e., images with a free center (pore) and metal in an off-center position. The eigenvectors #2 and 3, #4 and 5, and #6 and 7 represent characteristic pairs, each exhibiting similar densities rotated to each other by an angle related to the apparent rotational symmetry of the eigenimages. They describe one, two, or three noncentered cluster positions with arbitrary angular orientation. In principle, the importance images allow to quantify the maximum lateral displacements of cluster positions within the analyzed region. We find maximum off-center positions of clusters corresponding to a displacement radius of ≥2 nm. To illustrate

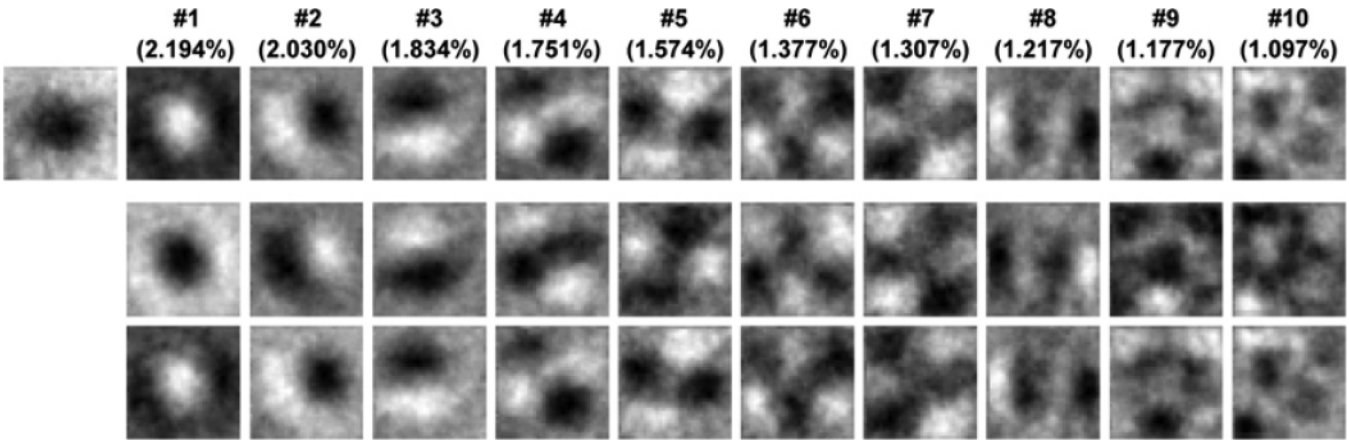

Figure 3. Principal component analysis of the 4 cluster sites A_1-A_4, located around the minor 4-fold symmetry axis (parts A and C of Figure 2). Upper row (#1−10): The 10 most significant eigenvectors sorted according to the size of the corresponding eigenvalues. They are displayed above the eigenimages and indicate the contribution of each eigenvector to the total variance. Dark and bright areas represent regions with maximum structural contrast. The image left to the eigenvectors is the average of the 1680 subareas analyzed, where the dark area indicates the mean position of Pd clusters. Middle and lower rows: Pairs of "importance images" calculated from the total average ± the corresponding eigenvectors displayed above. The importance images indicate the extreme situations of the variable structural detail with respect to the corresponding eigenvectors. Here, dark areas indicate contrast originating from Pd clusters, and bright areas are free of metal. Size of images 4.3 × 4.3 nm^2.

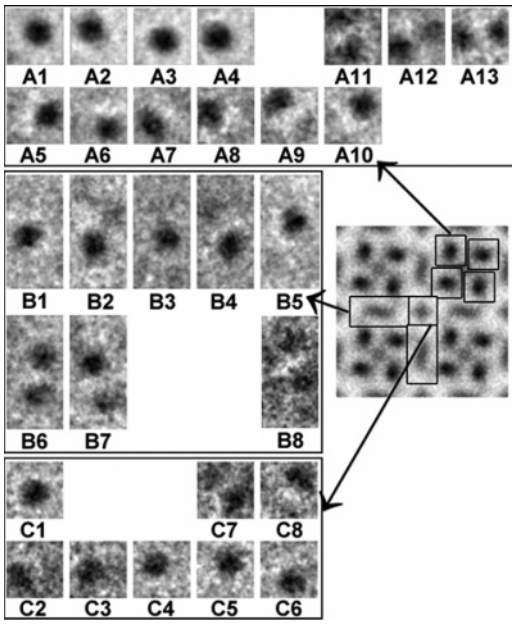

Figure 4. Averages of subsets of images after PCA and classification. The number of images contained in the classes A_1-A_{13}, B_1-B_8, and C_1-C_8 are given in Table 1. The images originate from the cluster sites A, B, and C as marked in the average displayed and in Figure 2. Dark areas indicate Pd clusters. Image size 4.3 × 4.3 nm^2 (class averages from cluster sites A and C) and 4.3 × 8.6 nm^2 (class averages from cluster site B).

the variation in cluster positioning more clearly, we used the results of PCA to separate the site A, B, and C images into more homogeneous subclasses.

3.4. Classification of Cluster Positions. For classification purposes, we projected the 1680 site A images into the seven-dimenisonal subspace defined by eigenvectors #1−7 (Figure 3) and grouped the images that were located together. The total number of classes was determined empirically. The number was increased as long as new classes showed detectable and structurally clearly interpretable differences to the previous ones. The images belonging to the cluster sites B and C were treated in a similar way. Figure 4 shows the averages of the final image classes A1−A13, B1−B8, and C1−C8, respectively. The corresponding number of images contributing to the classes are given in Table 1. The

Table 1. Number of Classified Images after Principal Component Analysis of the Subareas of Cluster Sites A, B, and C, Respectively

	cluster site		
class no.	A	B	C
1	193	124	45
2	182	116	78
3	222	50	26
4	190	53	59
5	129	110	46
6	126	98	49
7	92	180	62
8	83	109	55
9	103		
10	113		
11	84		
12	90		
13	73		
Σ	1680	840	420

local averages provide a rather realistic measure of the average Pd particle size, which is about 1.2−1.5 nm.

An interesting result is the high occupation number of the characteristic metallization sites. In about 85% of all cases, the four cluster sites at A are occupied by one cluster (classes A1−A10). Only 15% of the images were identified to contain either two separated Pd clusters (A11−A13) or less-defined structures. Although the eigenvectors of site A images also suggested the existence of three clusters per subarea (Figure 3), they did not show up in the class averages (Figure 4), indicating that this pattern is neither qualitatively nor quantitatively prominent. A similar result is obtained for cluster site C. Here, 72% of the images apparently contain a single cluster (C1−C6 and C8). A different situation was found for site B, where more than 46% of the images showed two or more Pd clusters.

The second important result from PCA is the clear variability of the individual cluster positions. According to classification, about 55% of the cluster positions (A1−A4) deviate from the pore center (corresponding to the image center) by a distance less than the cluster radius. The remaining 45% showed larger deviations. A similar situation is found for site C. For both sites, A and C, the local deviations are arbitrary in direction. This behavior is

particularly clearly visible in the class averages A5−A10, where a characteristic "sine-wave-like" positioning of clusters can be observed. Again, a different behavior is found for the clusters at site B. Here, the cluster positions along the elongated protein gap showed a higher variability than perpendicular to it (classes B1 to B7 in Figure 4).

While the existence of positional variability was a clear outcome of our analyses, it remained to be clarified whether the displacement was a genuine feature of Pd cluster deposition or whether it was artificially introduced by misalignment of unit cells in the course of cross correlation.

3.5. Genuine Cluster Variability or Displacement by Misalignment? Correlation averaging has the advantage that displacements of unit cells from ideal crystallographic positions can at least partly be corrected for. However, the precision of cross correlation depends on the signal-to-noise ratio that is rather low in micrographs of the metallized S layers (Figure 1) and on the structural variability of unit cells (see Materials and Methods). It is, thus, conceivable that the observed variability of cluster positions originates from alignment errors. In the following, we present evidence excluding a substantial contribution from simple misalignment.

(i) All three types of cluster sites contained not only one but also two or more clusters. This implies the existence of different cluster positions that cannot be explained by statistical misalignment. In addition, these cluster pairs occurred substantially rotated to each other (Figure 4, A_{11}−A_{13}), a situation which cannot be achieved by lateral misalignment of a 2D crystal.

(ii) If the variations of cluster positions originated from correlation errors, one would expect laterally isotropic displacements for all cluster sites. This is obviously not true for site B where the displacements along the elongated protein gap were larger than perpendicular to it. Accordingly, the statistical error should not exceed the offset of the symmetric arrangement of the cluster pairs from the gap center in the *x* direction in Figure 4 (B_6 and B_7). This offset accounts for 1−3 pixels on average, corresponding to 0.12−0.36 nm, while the radial displacements in the class averages A_5−A_{10} were in the range of 1−2 nm.

(iii) In a further approach, we performed PCA and subsequent classification of the four different A sites separately (Figure 2C, A_1−A_4) and compared the individual distributions of clusters. If we assume that the variability of cluster positions was predominantly an effect of misalignment, meaning that the clusters from each single unit cell were shifted into a particular direction, the cluster positions in the corresponding A sites should be correlated and should be statistically independent otherwise. To test this hypothesis we selected the images of each class of site A_1 and analyzed the class distributions of the corresponding clusters from the other A sites (see Materials and Methods). The clear result was that the distributions are independent from each other at a significance level of 5% according to the χ^2 tests.

To take the results together, we must conclude that the positional variability of the Pd clusters in the sites A, B, and C predominantly reflected genuine variations of cluster positions.

3.6. Binding of Multiple Nucleation Sites. To assess the metal−complex binding capacity of the S-layer protein, we incubated S-layer sheets in K_2PdCl_4 solution without adding reducing agents so that cluster growth was suppressed. After incubation the protein was removed by ultracentrifugation and the UV−vis spectrum determined from the supernatant to determine the remaining content of Pd complexes.[34] The results of several experiments showed characteristics as follows. (i) The complex concentration was clearly less in supernatants after 2−3 h incubation with the S-layer protein compared to control solutions. (ii) The spectra did not change further when the S layer had been removed, i.e., loss of complexes from the solution was dependent on the protein. (iii) Quantitative assessments suggested that about 200−300 complexes associated with one protein monomer, i.e., an amount of $\sim 10^3$ complexes/unit cell. Interestingly, the range is about 2 orders of magnitude higher than the number of Pd clusters/unit cell found.

4. Discussion

The cluster arrays grown by chemical reduction of Pd complexes in the presence of the regularly arrayed S-layer protein exhibited a pattern very similar to that obtained by electroless Pt deposition on the same target previously.[15] In both cases, the metal clusters occurred in 7 characteristic sites per unit cell with similar morphologies on average. The results presented here might, thus, also apply for metallization with Pt. Correlation averaging revealed clear evidence for preferred cluster sites close to the two 4-fold and at the 2-fold symmetry axes, although the local precision of deposition was disturbed by considerable variability of hitherto unknown source. The Pd clusters are located within or close to the pores and gaps of the S-layer framework as illustrated by its 3D structure.[26] This finding apparently supported the view of a template-directed growth of metal particles on S-layer proteins by reductive cluster formation.[15] However, PCA provided deeper insight. On the basis of individual PCA of the three cluster sites A, B, and C, we were able to describe the distinct distributions of cluster positions and to derive characteristic features such as (i) the cluster size, (ii) the occupation probability of metallization sites, and (iii) the inherent variability of cluster positions within these sites.

The Pd clusters had a characteristic size of 1.2 to about 1.5 nm independent of the localization in a certain cluster area. They were, thus, smaller than the Pt clusters on the same S layer showing a diameter of 1.9 nm on average obtained under similar conditions.[15] Since Pd and Pt have almost identical atomic volumes and occur in the same crystalline packing the Pd clusters contained less atoms in the characteristic case. The enhanced growth of Pt clusters remains to be investigated, but it is conceivable that the higher electron affinity of Pt is of some influence.

Although the contrast variations of the cluster sites did not suggest a high occupation of particles at the first glance, PCA revealed that apparently every image of all the sites showed metal contrast. About 85% of the 4 cluster sites around the symmetry axes A were loaded by one cluster each, the remaining 15% either contained two separated Pd clusters or less-defined structures. However, neither of the cluster

sites was found to be free of particles, and none of the more significant eigenvectors suggested a clear contribution of images without any contrast from metal. So, metallization of the preferred sites was apparently complete. This conclusion is in agreement with the total number of individual clusters directly counted in a larger S-layer area. Here, we found about eight clusters per unit cell area.[34]

But may we regard a "site" as being highly occupied if the cluster positions vary considerably? About 55% of the A sites with a single Pd particle showed cluster positions that were displaced from the pore center in arbitrary direction by a distance less than the cluster radius. This distance is too small to allow the deposition or growth of additional clusters near the center. So, in about half of all cases, the 4 A site pores are loaded with clusters located rather "specifically" in the center and closely surrounded by the protein surface forming the pores. The remaining A sites were occupied by one or more particles located at the "rim" or the pore wall. These clusters were randomly distributed with respect to the pore center, indicating that there is no locally defined nucleation center for cluster growth. A distinct behavior was observed for site B clusters where half of the elongated protein gaps contained two or more particles. Obviously, steric hindrance was not a problem. And we found that the variation of cluster positions was biased by the geometry of the gap and was not arbitrary in direction, the cluster positions varied much more along the protein gap than perpendicular to it. The comparison between the characteristic features of the sites A and B clearly demonstrates the direct influence of the protein morphology on both occupation and variability of individual cluster positions, supporting the hypothesis of a template-directed growth of Pd clusters at the S layer surface.

However, is it possible to derive a more detailed view of the local interactions in the process of nucleation and growth of metal clusters? The intriguing problem is whether the local templating effect is chemically based, e.g., driven by the chemical potential between the metal complexes and the local amino acid residues, or rather physically based, i.e., effected by the geometry of the S layer.

Recently, we studied the conditions for selective nucleation and growth of Pt and Pd clusters at DNA, both experimentally[13,42−44] and theoretically.[13,45] The key for reductive metallization is the incubation of DNA with an aged metal salt solution to allow the binding of hydrolyzed metal complexes. The latter act, in the subsequent reduction step, as preferential nucleation centers for the selectively heterogeneous cluster growth.[13,42] Our investigations by first-principles molecular dynamics revealed that the nucleotide ligands both enhance the electron affinity of the complexes and stabilize the formation of Pt−Pt bonds during the first reduction steps.[13,45] Cluster growth is an autocatalytic process, and the first-formed nuclei quickly develop to larger clusters, consuming the dissolved metal complexes. In this way, the delicate balance between the kinetics of reduction in the homogeneous and heterogeneous nucleation and growth channels is shifted toward the heterogeneous growth of clusters at the template. Since this reaction involves covalent binding of metal complexes to specific DNA bases, metallization is mainly determined by the local chemistry of the metal−complex−DNA adducts.

Theoretical considerations suggest that this mechanism also works for amino acids acting as electron donors, i.e., particularly for histidine containing an imidazole ring.[45,46] Nevertheless, the same process is not likely to occur with S layers because they usually do not possess many amino acids that could function as electron donors. The relative content of histidine, cysteine, and tryptophan in the S layer of *S. ureae* is approximately 0.6, 0, and 0.9% of all amino acids, accounting for about eight histidine residues (of unknown location) per monomer.[47] This is in contrast to the relatively high number of Pd complexes bound to the protein. Therefore, binding of metal complexes to the S layer cannot depend on the presence of rare reducing amino acids. It is likely that the metal complexes are immobilized by various amino acid residues or abundant groups that are located on the surface of S-layer proteins and in the preferred metallization sites in particular.

Therefore, we propose a model for the heterogeneous nucleation and growth of Pd (and Pt) clusters on protein surfaces, which is based on the mechanism of heterogeneous nucleation described in refs 13 and 45 with the important difference that amino acid residues are not necessarily directly involved in the reduction process. The essential steps for cluster formation are (i) binding of metal complexes to the protein surface via still unresolved (e.g., polar) interactions, (ii) formation of a surface-associated Pd nucleation site by a reducing agent, (iii) autocatalytic cluster growth consuming (a) locally enriched (surface associated) complexes or closely located clusters in the early state of development and thereby attenuating competitive cluster growth in the very neighborhood, and (b) complexes from the bulk solution. In fact, metal complexes associated on the surface are available at a much higher density than those from the bulk. Given that $\sim 10^3$ complexes are bound to one unit cell, about 3 complexes/nm^2 can be expected on the (projected) surface area (of both sides of the S-layer sheet), while 3 soluble complexes populate a bulk solution volume of $12.9 \times 12.9 \times 10$ nm^3 next to the S-layer surface with the actual experimental conditions (12.9 nm corresponds to the unit cell size). The characteristic distance between surface-associated complexes is, thus, considerably smaller, and they are more easily available for initial cluster growth. Up to 30% of the Pd contained in the final clusters may originate from surface-bound complexes. Nucleation sites situated in areas with an enhanced density of surface-associated complexes will preferably grow and finally occupy the metallization site. If none of the bound complexes is

(42) Seidel, R.; Mertig, M.; Pompe, W. *Surf. Interface Anal.* **2002**, *33*, 151.
(43) Mertig, M.; Seidel, R.; Colombi Ciacchi, L.; Pompe, W. *AIP Conf. Proc.* **2002**, *633*, 449.
(44) Seidel, R.; Colombi Ciacchi, L.; Weigel, M.; Pompe, W.; Mertig, M. *J. Phys. Chem. B* **2004**, *108*, 10801.
(45) Colombi Ciacchi, L.; Mertig, M.; Seidel, R.; Pompe, W.; De Vita, A. *Nanotechnology* **2003**, *14*, 840.
(46) Colombi Ciacchi, L.; Mertig, M.; Pompe, W.; Meriani, S.; De Vita, A. *Platinum Metals Rev.* **2003**, *47*, 98.
(47) Beveridge, T. J. *J. Bacteriol.* **1979**, *139*, 1039.

distinguished as a particular nucleation site, the final position of clusters will vary, corresponding to the results obtained.

Under these conditions, the observed cluster positions can also be regarded in analogy to the behavior of adatoms on vicinal surfaces. Here, two characteristic positions are energetically favored. The early studies by Brassett and Bethge showed that step ledges are preferred nucleation sites for adatoms because of the increasing coordination with respect to the terrace sites.[48,49] Later Ehrlich[50] and Schwoebel[51] showed that adatoms also locate preferentially on the upper terrace step due to the occurrence of a diffusion barrier down from the terraces. In analogy, favored types of cluster positions at the S-layer surface are the pores, where metal clusters experience a maximum of contact area with the protein, and the rims or walls of the pores. It is well conceivable that clusters grown in areas where they could develop multiple contacts to the protein surface were more stable in position than those at exposed areas and less interaction with the protein surface. As a consequence, complexes will be found enriched in surface regions with cavities, pores, and gaps.

In conclusion, we demonstrated that Pd clusters grown on a 2D protein crystal by chemical reduction, first, were variable in position very likely due to multiple nucleation sites bound to the protein. The initial steps of cluster formation can be explained by a model of heterogeneous Pd complex reduction and creation of nucleation sites, which includes binding of metal complexes to more common groups of amino acids, possibly enriched in subareas of the protein surface. We, second, showed that the Pd clusters were preferably located in porous regions of the protein lattice, providing sufficient or maximum cluster−protein interactions and, thus, stabilizing the cluster positions. This is a rather physically based contribution of the protein structure and a distinguished property of S layers.

There is great interest in the controlled deposition of functional molecules and inorganic particles on nanoscopically structured surfaces and polymeric material.[1,52] To develop specific methods for this purpose, we need to understand the interaction between inorganic clusters, functional molecules and organic templates in more detail. The results of our investigations presented here help to address important questions to achieve this goal. The challenge for the future is to elucidate the mechanism of complex binding and to control the nucleation process as to metallize protein or DNA templates more specifically.

Acknowledgment. We thank Manfred Bobeth for fruitful discussions. This work was supported by the DFG (Grants PO392/18 and En144/3), the BMBF (Grant 13N8145), the SMWK, and the EU (FP5, Contract G5RD-CT-2002-0750).

CM048497P

(48) Bassett, G. A. *Philos. Mag.* **1958**, *3*, 1042.
(49) Bethge, H. *Surf. Sci.* **1964**, *3*, 33.
(50) Ehrlich, G.; Hudda, F. G. *J. Chem. Phys.* **1966**, *44*, 1039.
(51) Schwoebel, R. L.; Shipsey, E. J. *J. Appl. Phys.* **1966**, *37*, 3682.
(52) Le, J. D.; Pinto, Y.; Seeman, N. C.; Musier-Forsyth, K.; Taton, T. A.; Kiehl, R. A. *Nano Lett.* **2004**, *4*, 2343.